12-1999

WIYN Open Cluster Study. II. UBVRI CCD Photometry of the Open Cluster NGC 188

Ata Sarajedini
Wesleyan University

Ted von Hippel
Embry-Riddle Aeronautical University, vonhippt@erau.edu

Vera Kozhurina-Platais
Yale University, vera@astro.yale.edu

Pierre Demarque
Yale University, demarque@astro.yale.edu

THE ASTRONOMICAL JOURNAL, 118:2894–2907, 1999 December

WIYN OPEN CLUSTER STUDY. II. *UBVRI* CCD PHOTOMETRY OF THE OPEN CLUSTER NGC 188

ATA SARAJEDINI
Department of Astronomy, Wesleyan University, Middletown, CT 06457; ata@astro.wesleyan.edu
TED VON HIPPEL
Gemini Observatory, 670 A'ohoku Place, Hilo, HI 96720; ted@gemini.edu
VERA KOZHURINA-PLATAIS
Department of Astronomy, Yale University, New Haven, CT 06520; vera@astro.yale.edu
AND
PIERRE DEMARQUE
Department of Astronomy, Yale University, New Haven, CT 06520; demarque@astro.yale.edu
Received 1999 July 21; accepted 1999 August 17

ABSTRACT

We present high-precision *UBVRI* CCD photometry of the old open cluster NGC 188. Our color-magnitude diagram extends from near the red giant branch tip to as faint as ~ 5 mag below the main-sequence turnoff. From an analysis of these data along with published photometry for M67, we draw the following conclusions: (1) From the *UBV* two-color diagram, we find a reddening of $E(B-V) = 0.04 \pm 0.02$ for M67 and $E(B-V) = 0.09 \pm 0.02$ for NGC 188. (2) Based on main-sequence fitting to solar abundance isochrones, the distance moduli turn out to be $(m-M)_v = 9.69 \pm 0.11$ for M67 and $(m-M)_v = 11.44 \pm 0.08$ for NGC 188. (3) The comparison of the CMDs to theoretical isochrones indicates that an amount of core convective overshoot equivalent to 0.10 of a pressure scale height is appropriate for M67, while no overshoot is required to fit the CMD of NGC 188. These isochrones suggest that NGC 188 is 3.0 ± 0.7 Gyr older than M67. (4) There is a clear indication of mass segregation in both M67 and NGC 188, with the most massive stars ($M/M_\odot > 1.1$) being more centrally concentrated than those that are the least massive ($0.8 \geq M/M_\odot > 0.65$).

Key words: galaxies: formation — galaxies: star clusters

1. INTRODUCTION

Studying the properties of open star clusters holds great promise in answering a number of long-standing astrophysical questions. As stellar laboratories, open clusters allow us to modify and refine theoretical models that describe the properties of stars. Younger clusters are primarily useful in constraining models of star formation and progressively older clusters are important contributors to our understanding of how stars evolve, as well as the end states of stars. As probes of Galactic structure, open clusters trace the formation and evolution of the disk. The sheer number of open clusters and their extensive distribution throughout the disk (and outside it) mean that they provide both a spatial and temporal record of the conditions in the Galactic disk.

The importance of open clusters, as outlined above, has lead to the formation of the WIYN Open Cluster Study (WOCS) collaboration described in von Hippel & Sarajedini (1998, hereafter Paper I). Our highest priority target is the old cluster NGC 188. For a long time, NGC 188 was considered to be the oldest open cluster in the Galactic disk. Sandage (1962) first derived the age of 14–16 Gyr on the basis of Hoyle's (1959) stellar models. Since then, age estimates of NGC 188 have ranged from 5 Gyr (Demarque & McClure 1977; Twarog 1978) to 9–12 Gyr (Demarque & Larson 1964; Iben 1967), with the most recent value being closer to 6 Gyr (Caputo et al. 1990). However, in recent years, NGC 188 has relinquished the title of oldest open cluster to NGC 6791, which is 8 Gyr old (Chaboyer, Green, & Liebert 1999, and references therein) and is the oldest disk cluster, and to Berkeley 17, which is 12 Gyr old and located some 160 pc below the Galactic disk (Phelps 1997).

In Paper I we presented a deep *VI* color-magnitude diagram (CMD) for NGC 188 and used it to study the reddening and distance modulus of the cluster as well as the phenomenon of mass segregation and the white dwarf population. In addition, we found that our *V* photometry was 0.05 ± 0.01 mag fainter relative to that of Eggen & Sandage (1969). Because all published CMDs of NGC 188 before Paper I had used the scale of Eggen & Sandage for calibration, this difference was rather disturbing, thereby underscoring the importance of settling this discrepancy in the photometric scales.

As the next paper in the WOCS series, we present, herein, a more complete, though not as deep, photometric data set for NGC 188 in the *UBVRI* filter passbands. In order to place our results on a firmer foundation and in the proper context, we have chosen to perform the analysis of NGC 188 with respect to the nearly solar age and abundance open cluster M67. Our aim is twofold. First, we will utilize the clusters' color-magnitude diagrams (CMDs) to determine values of reddening, distance, and age. Second, the distribution of main-sequence stars in these clusters will be used to study the phenomenon of mass segregation and its relation to cluster age. The next two sections describe the observations of NGC 188 and how they were reduced. Section 4 presents the main results of this investigation including the CMD, isochrone fits, and an analysis of mass segregation in the cluster. The conclusions are summarized in the last section.

2. OBSERVATIONS

The observations of NGC 188 were obtained during two separate runs on the 0.9 m telescope at Kitt Peak National

TABLE 1

JOURNAL OF OBSERVATIONS

Civil Date	Filter	Exposure (s)	Air Mass	Photometric?
1995 Sep 13.....	*B*	3 × 18	1.7	N
	B	3 × 180	1.7	N
	V	3 × 12	1.7	N
	V	3 × 120	1.7	N
	I	2 × 15	1.7	N
	I	1 × 40	1.7	N
	I	1 × 120	1.7	N
	I	2 × 400	1.7	N
1996 Oct 21.....	*U*	2 × 100	1.8	N
	B	2 × 30	1.8	N
	V	2 × 20	1.8	N
	R	2 × 15	1.8	N
	I	2 × 40	1.8	N
1996 Oct 22.....	*U*	1 × 200	1.8	Y
	U	1 × 100	1.8	Y
	B	1 × 60	1.8	Y
	B	1 × 30	1.8	Y
	i	1 × 40	1.8	Y
	V	1 × 20	1.8	Y
	R	1 × 40	1.8	Y
	R	1 × 15	1.8	Y
	I	2 × 40	1.8	Y

Observatory using the f/7.5 secondary. Table 1 shows the log of the observations. In all cases, a 2048 × 2048 pixel Tektronix CCD (T2KA) was used producing an image scale of 0.″68 pixel^{-1} and a field of view of 23′ × 23′ centered on the cluster. In order to minimize errors due to flat-fielding and cosmetic defects, the telescope was offset slightly between exposures. In general, twilight sky flats were used to flat-field these observations. However, in a few cases, where adequate sky flats did not exist, dome flats were used to account for the pixel-to-pixel sensitivity variations and smoothed sky flats were then applied for the illumination correction.

On the one photometric night (1996 October 22), we observed 38 standard stars drawn from the list of Landolt (1992). These stars had a color range of $-0.2 \leq (B-V) \leq 1.5$ and were observed at air masses as high as 1.9.

3. REDUCTIONS

3.1. *Standard Stars*

The equations that form the photometric calibration used in this paper are the following:

$$u = U + a_U + b_U(B-V) + bb_U(B-V)^2 + c_U X_U\,, \quad (1)$$

$$b = B + a_B + b_B(B-V) + c_B X_B\,, \quad (2)$$

$$v = V + a_V + b_V(B-V) + c_V X_V\,, \quad (3)$$

$$v = V + a'_V + b'_V(V-R) + c_V X_V\,, \quad (4)$$

$$v = V + a''_V + b''_V(V-I) + c_V X_V\,, \quad (5)$$

$$r = R + a_R + b_R(V-R) + c_R X_R\,, \quad (6)$$

$$i = I + a_I + b_I(V-I) + c_I X_V + d_I UT_I + e_I UT_I^2\,. \quad (7)$$

In this formulation, the lower case letters represent the instrumental magnitudes corrected for exposure time, the upper case symbols indicate magnitudes on the standard system, and X is the air mass of each observation. Each equation contains at least a zero point, a linear color term, and an extinction term. In addition to this, equation (1) required a quadratic color term and equation (7) required both a linear and quadratic UT term to eliminate significant trends in the residuals. The rms deviations of the standard values from the fits were 0.034 mag in equation (1), 0.015 mag in equation (2), 0.013 mag in equation (3), 0.013 mag in equation (4), 0.012 mag in equation (5), 0.011 mag in equation (6), and 0.014 mag in equation (7). We have chosen to parameterize the U magnitude in terms of the $B-V$ color as opposed to the more traditional $U-B$ color. This is because the former allows one to perform a satisfactory fit utilizing low powers of the color term, whereas the latter often requires higher order color terms to adequately model the variation of the residuals with color (Sarajedini et al. 1995b).

3.2. *Cluster Frames*

The cluster frames were reduced using the DAOPHOT II photometry package (Stetson 1994) in the same manner as described by Sarajedini & Milone (1995). In summary, on each of the 38 CCD frames, between 100 and 200 uncrowded stars were used to construct a high signal-to-noise point spread function (PSF). This PSF was then fitted to all detected profiles on each frame under the constraint that its shape vary quadratically across the frame. Two iterations of FIND, PHOTOMETRY, and ALLSTAR II were applied to each image, and the final subtracted frames were inspected to be sure that all well-exposed but unsaturated stars had been detected.

The next step involved the determination of aperture corrections for each frame. To facilitate this, between 100 and 200 bright stars were selected and all remaining stars were subtracted from each frame. Apertures containing more than 99% of the light were placed on each star and a total magnitude was measured. The difference between this total magnitude and the PSF magnitude is then the aperture correction. In some cases, we found that the aperture correction varied with position on the frame. We were able to model this variation analytically using low-order polynomials (see Paper I). Typical standard errors of the mean for the aperture corrections were less than 0.01 mag.

The final instrumental magnitudes were edited using the image diagnostics computed by DAOPHOT (see Sarajedini & Da Costa 1991) and matched up to form colors. The data obtained under photometric conditions (1996 October 22) were transformed to the standard system using equations (1)–(7) yielding a master list of transformed data. The non-photometric data were then calibrated using color terms and zero points derived from stars in common between the two data sets. The numbers of stars used in this procedure ranged from 150 to 800, while the rms deviations of the fits ranged from 0.009 to 0.032 mag.

3.3. *Comparison With Previous Photometry*

As discussed in Paper I, much of the published photometry of NGC 188 has been calibrated to the system of Sandage (1962) and Eggen & Sandage (1969, hereafter ES69). The WIYN telescope data from Paper I was based on an independent calibration that showed a serious discrepancy relative to the ES69 data. In particular, we found $V(\mathrm{ES69}) - V(\mathrm{Paper\ I}) = -0.052 \pm 0.007$, which is a highly significant difference.

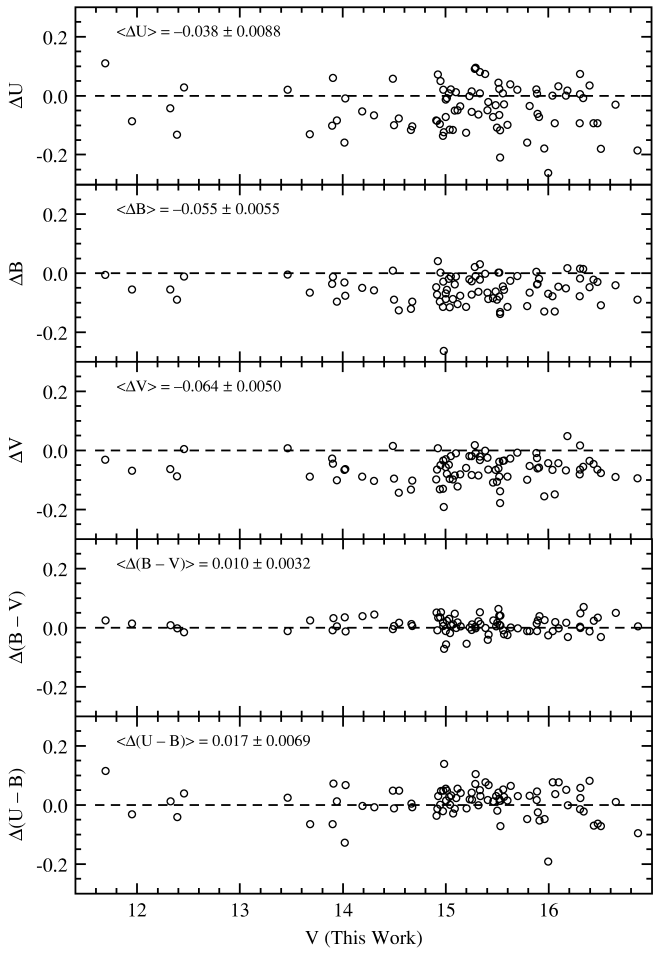

FIG. 1.—Star-by-star comparison of our photometry for NGC 188 with the photoelectric data of Eggen & Sandage in the sense (ES69 minus this work). The median offsets are given in each panel. Note that, while the individual magnitude offsets are quite significant, the color differences are much less so.

We can perform the same experiment with the data presented herein. Figure 1 shows such a comparison where we plot the UBV magnitude difference as a function of the V magnitude from the present study. We find $\Delta U = -0.038 \pm 0.0088$, $\Delta B = -0.055 \pm 0.0055$, $\Delta V = -0.064 \pm 0.0050$, $\Delta(B-V) = 0.010 \pm 0.0032$, and $\Delta(U-B) = 0.017 \pm 0.0069$, where the differences are in the sense (ES69 minus this work). This is consistent with the findings of Paper I, thus supporting the robustness of the calibration used in Paper I. In addition, we find the following photometric offsets relative to the results of Paper I: $\Delta V = -0.015 \pm 0.0017$ and $\Delta I = -0.002 \pm 0.0010$. Keeping in mind that the photometric calibration used here and that utilized in Paper I are each based on only one photometric night, the actual differences between them are gratifyingly small and within the expected uncertainties of the standard star calibrations.

To illustrate a comparison between our NGC 188 data and previously published CCD photometry, we show, in Figure 2, our BV CMD along with those of Caputo et al. (1990) and Kaluzny 1990). From inspection of these diagrams, it is clear that the present NGC 188 photometry represents a marked improvement over existing data. In particular, the improvements have come in the following areas: (1) our photometric scale appears to be more robust (recall that both Caputo et al. and Kaluzny calibrated their data to the scale of ES69), (2) our CMD shows better definition of the cluster's principal sequences, and (3) we have imaged more of the cluster than previous CCD studies.

4. RESULTS AND DISCUSSION

4.1. *Color-Magnitude Diagrams*

The four panels of Figure 3 show the color-magnitude diagrams (CMDs) of NGC 188 in the $U-B$, $B-V$, $V-I$, and $U-I$ passbands. We see that our photometry extends from near the red giant branch tip to as faint as ~ 5 mag below the main-sequence turnoff. There is a well-defined main-sequence, subgiant branch, and red giant branch, though the helium burning clump is sparsely populated; to the extent that we can isolate the clump, it appears to be composed of three stars at $V = 12.43$. There are also three hot subdwarf stars that are exceptionally blue and most obvious in the $V-I$ and $U-I$ CMDs. Their photometric properties are listed in Table 2. Landsman et al. (1998) provide a discussion of Ultraviolet Imaging Telescope (UIT) observations of these three stars. It turns out that the photometry in Table 2 is the first such optical data measured for UIT-1.

As is the case with the deep CMD published in Paper I, this shallower CMD also displays a prominent sequence of equal mass binaries (0.75 mag above the main sequence) most obvious in the $V-I$ CMD. In the next sections, we proceed in a systematic manner to determine the basic cluster properties such as reddening, distance, and age. Throughout this entire discussion, we have adopted a metal abundance of [Fe/H] $= -0.04 \pm 0.05$ for NGC 188 (Paper I), [Fe/H] $= -0.05 \pm 0.08$ for M67 (Montgomery, Marchall, & Janes 1993), and [Fe/H] $= 0.13 \pm 0.05$ for the Hyades (Boesgaard & Friel 1990).

4.2. *Reddening*

Before presenting the analysis of NGC 188's reddening, we need to discuss the relations between reddening and extinction in the various filter passbands used in this study. For these, we rely on the results of Cardelli, Clayton, & Mathis (1989). When transformed to the central wavelengths of the specific filters we used, the general relations of Cardelli et al. (1989) become

$$A_U = 4.86E(B-V)\,, \quad A_B = 4.18E(B-V)\,,$$
$$A_I = 1.74E(B-V)\,, \tag{8}$$
$$E(U-B) = 0.68E(B-V)\,, \quad E(V-I) = 1.43E(B-V)\,,$$
$$E(U-I) = 3.12E(B-V)\,. \tag{9}$$

These are based on the assumption that $A_V = 3.1E(B-V)$. We note in passing that in Paper I, we adopted $E(V-I) = 1.34E(B-V)$; the difference is solely based on the fact that the I filter used in Paper I was centered slightly bluer than the one used herein.

TABLE 2

SUBDWARF O/B STARS

Star	V	$U-B$	$B-V$	$V-I$
D-702.....	14.18	−0.28	0.28	0.40
II-91	16.27	−0.51	−0.14	−0.15
UIT-1.....	18.46	−1.04	0.03	−0.60

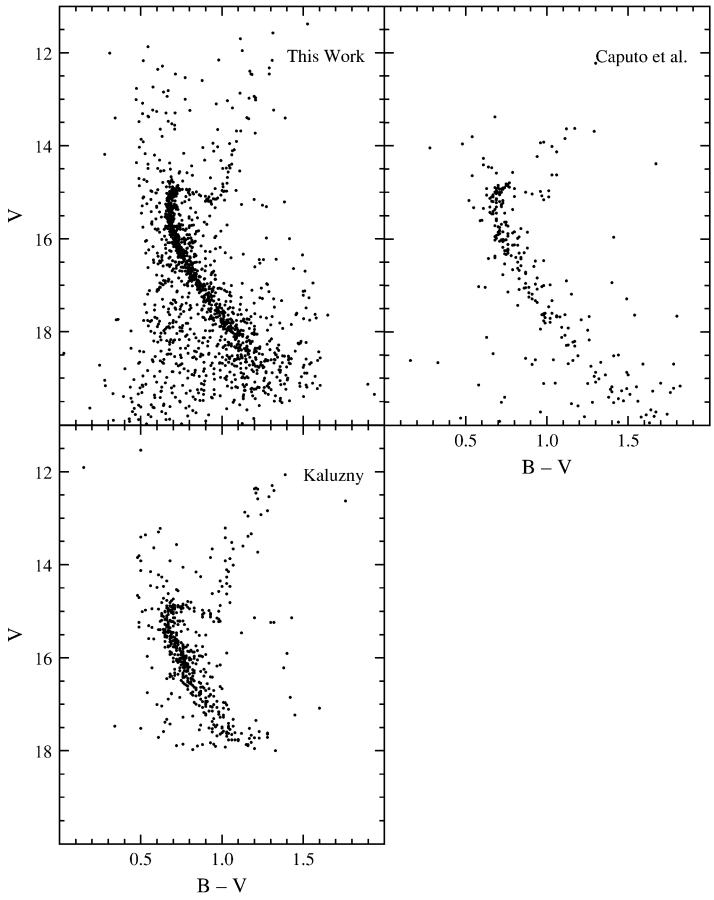

FIG. 2.—Side-by-side comparison of our CCD BV photometry for NGC 188 with those of Caputo et al. (1990) and Kaluzny (1990). It is clear that the photometry presented in this work represents a marked improvement over previous data.

To facilitate our differential study of NGC 188 relative to the well-known near solar age and metallicity open cluster M67, we begin by measuring the reddening of M67. Montgomery et al. (1993) have utilized the UBV two-color diagram and the fiducial sequence of the Hyades (Schmidt-Kaler 1982) to estimate a reddening of $E(B-V) = 0.05 \pm 0.01$ for M67. We have redone this using their photometric data, and the result is shown in the left panel of Figure 4. Indeed a shift of 0.05 mag in $(B-V)$ and a corresponding shift of 0.034 mag in $(U-B)$ minimizes the rms residuals between the individual M67 main-sequence stars and the Hyades locus. This is also shown in Figure 11 of Montgomery et al. (1993). However, we must include a correction for the metallicity difference between M67 and the Hyades. The Yale Isochrones indicate that a correction of 0.07 mag dex^{-1} in $E(B-V)$ must be subtracted from our derived reddening to account for this abundance difference.[1] As a result, we arrive at a reddening of $E(B-V) = 0.04 \pm 0.02$, where the quoted uncertainty includes an estimate of the error in the reddening determination as well as the additional error in the correction for abundance. The same procedure applied to NGC 188 yields an optimum reddening of $E(B-V) = 0.09 \pm 0.02$, as shown in the right panel of Figure 4. This is in excellent agreement with the value estimated in Paper I of $E(B-V) = 0.09$. Furthermore, the dust maps of Schlegel, Finkbeiner, & Davis (1998) indicate reddenings of $E(B-V) = 0.03$ and $E(B-V) = 0.09$, at the positions of M67 and NGC 188, respectively, both of which are in accord with our values. All in all, it appears that we have settled on robust reddening values for M67 and NGC 188.

4.3. *Distance*

Since we will eventually want to compare the CMDs of M67 and NGC 188 to isochrones to estimate the cluster ages, we will determine the distances using the unevolved main sequence provided by the isochrones (discussed in the next section).

After registering the cluster photometry in color based on the reddenings measured in the previous section, we shift the data in magnitude until the main sequence of the $B-V$ isochrones matches that of the observational data; that is to say, we minimize the rms residuals between the individual cluster main-sequence stars and the isochrones in the color range $0.85 < (B-V)_0 < 1.0$. One must exercise caution when interpreting the results of this procedure because the influence of binary stars could produce a systematic bias in the resultant distance modulus. To test for this effect, we constructed histograms of the cluster main sequences in the color and magnitude directions. If the influence of binaries were significant, these histograms should display an asymmetric appearance around zero. In reality, all four histograms appear highly symmetric as evidenced by the fact that Gaussian fits reproduce the distributions quite well.

[1] See Demarque, P., Chaboyer, B., Guenther, D., Pinsonneault, M, Pinsonneault, L., & Yi, S. 1996 at http://shemesh.gsfc.nasa.gov/iso.html.

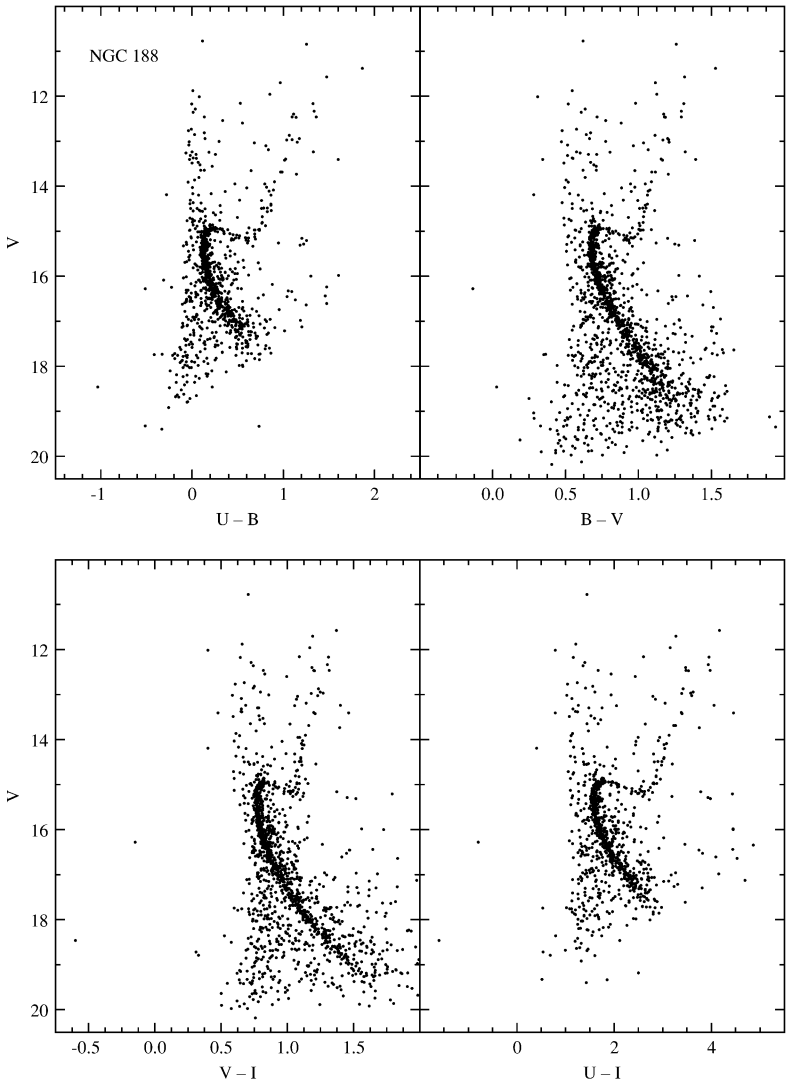

FIG. 3.—Four panels of this figure show our $U-B$, $B-V$, $V-I$, and $U-I$ color-magnitude diagrams of NGC 188. Note the three blue subdwarf stars that are members of NGC 188. Their visible light photometric data are listed in Table 2, while their ultraviolet properties have been studied by Landsman et al. (1998).

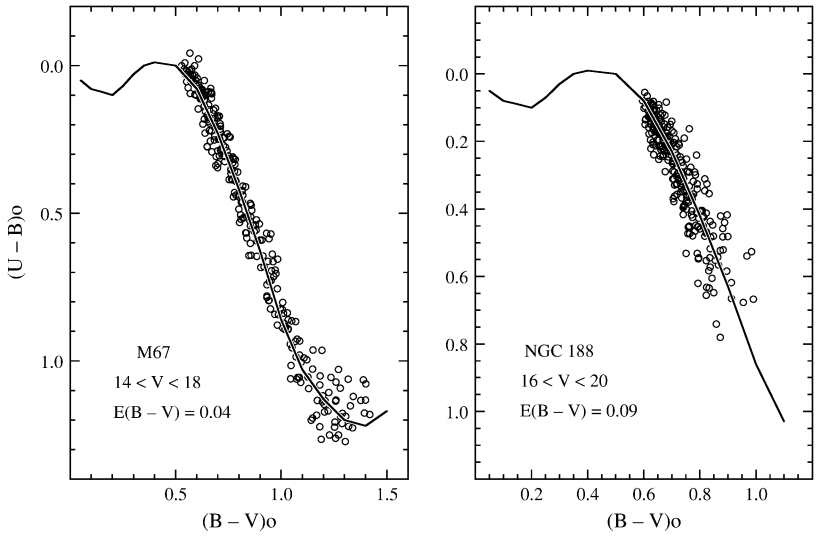

FIG. 4.—Left panel shows the two-color diagram for main-sequence stars in M67 from the photometry of Montgomery et al. (1993). The solid line is the Hyades main-sequence from Schmidt-Kaler (1982). The right panel illustrates the two-color data for main-sequence stars in NGC 188 using our photometry. When corrected for the metallicity differences between M67/NGC 188 and the Hyades, the color shifts required to impose coincidence on the cluster sequences yield the reddenings indicated in each panel.

This indicates that the width of the unevolved main sequence is not due to the presence of binary stars. Rather, it is predominantly a result of photometric errors in color, which are multiplied by the slope of the main sequence (~ 5) to produce the observed width.

Therefore, this procedure yields distance moduli of $(m - M)_v = 9.69 \pm 0.11$ for M67 and $(m - M)_v = 11.44 \pm 0.08$ for NGC 188. The quoted errors represent the addition in quadrature of (1) the estimated uncertainty inherent in the minimization process (± 0.01), (2) the uncertainty associated with the choice of stars as members of the main sequence (± 0.05), and (3) the influence of errors in the clusters' metal abundance (± 0.06 for NGC 188 and ± 0.10 for M67; see Paper I). We note in passing that these distances are based on the assumption that both NGC 188 and M67 have solar metal abundances. However, as mentioned in § 4.1, we have adopted slightly lower than solar metallicities for these clusters. The Yale isochrones indicate that $+0.044$ mag and $+0.055$ mag must be subtracted from the distance moduli of NGC 188 and M67, respectively, to account for their lower-than-solar metallicities.[2] We will not make this correction however because the cluster metallicities are solar to within the errors and because we are interested in determining the ages of these clusters by comparing to solar abundance isochrones.

In Paper I we presented a summary of previous distance estimates for NGC 188. In addition, we determined a new value of $(m - M)_v = 11.43 \pm 0.08$ under the assumption of solar metallicity, which turns out to be in excellent agreement with the distance modulus presented herein. In the case of M67, Montgomery et al. (1993) find a value of $(m - M)_v = 9.60$, which agrees with our value to within the errors.

4.4. *Direct CMD Comparisons*

Since we have derived values for the reddening and distance to M67 and NGC 188, we are in a good position to compare their CMDs in the absolute magnitude–intrinsic color plane. Figure 5 shows the $[M_V, (B-V)_0]$ and $[M_I, (V-I)_0]$ diagrams for M67 and NGC 188 superimposed on each other. It is reassuring that the unevolved main sequences of the two clusters are perfectly aligned in the two diagrams, and the relative positions of the main-sequence turnoffs reflect the age difference between them.

As predicted by the theoretical models of core helium burning red clump stars (Seidel, Demarque, & Weinberg 1987); Vassiliadis & Wood 1993; Sarajedini et al. 1995a; Alves & Sarajedini 1999), the M_V of the M67 red clump appears to be brighter than that of NGC 188; it is important to keep in mind however that the NGC 188 red clump is composed of only three stars. In any case, the current controversy over the sensitivity of the red clump magnitude to metallicity and age (Cole 1998; Udalski 1998) could be resolved once all of the target clusters in the WOCS project are reduced and analyzed together (Sarajedini 1999).

Last, we consider the relative positions of the cluster red giant branches (RGBs). In the range $1.5 < M_V < 2.5$, the average color difference between the M67 and NGC 188 RGBs is ~ 0.05 mag in $B-V$. The RGB color difference from the theoretical isochrones (discussed in the next section) is $\Delta(B-V) \sim 0.05$ indicating good agreement with the observational value.

4.5. *Fits to Theoretical Isochrones*

4.5.1. *Description of the Models*

As we discussed in § 4.1, the metallicities for NGC 188 and for M67 are very close to the solar value; thus we used the theoretical isochrones derived by Kozhurina-Platais et al. (1997) with an adopted value of $Z = 0.0188$, which corresponds to [Fe/H] = 0.00. This set of isochrones was calculated using the Yale Rotating Evolution Code (YREC) in its nonrotating mode for a standard stellar model calibrated to the Sun. Models were computed with different amounts of convective overshoot at the edge of the convective core, namely, $D_{\rm mix} = 0.0$, 0.15, 0.20, and $0.25H_p$, where H_p represents the pressure scale height at the core edge. Furthermore, we also constructed an additional set of isochrones for $D_{\rm mix} = 0.10H_p$ specifically for the present study.

[2] See http://shemesh.gsfc.nasa.gov/iso.html.

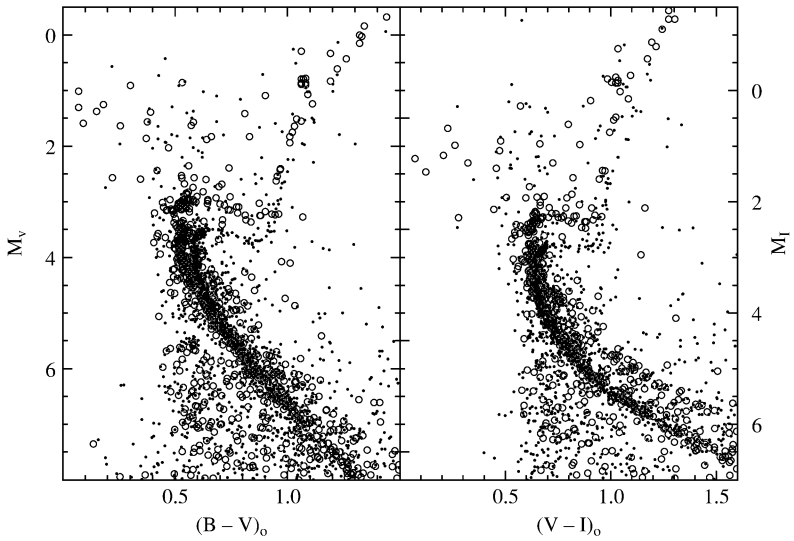

FIG. 5.—Left panel shows the $[M_V, (B-V)_0]$ color-magnitude diagram of M67 (*open circles*) and NGC 188 (*filled points*) constructed using the measured reddenings and distance moduli as described in the text. The right panel is the corresponding $[M_I, (V-I)_0]$ color-magnitude diagram. As noted in the text, all of the principal sequences in these diagrams are properly positioned relative to each other given the cluster metallicities and ages.

In order to achieve self-consistency in the stellar models, the parameters have to be calibrated to the Sun. In other words, the model's luminosity and radius at the age of the Sun should be as close as possible to the observed values of $L_\odot$ and $R_\odot$. Thus the final adopted values of $Y_\odot = 0.28242$ and $\alpha = 1.6674$—the mixing-length parameter that sets the efficiency of convective energy transport in the external layers of a star—produced the following model properties: (1) $X = 0.69878$, (2) $L/L_\odot = 1.000004$, (3) $R/R_\odot = 1.000086$, and (4) $\log(T_{\rm eff}) = 3.7618$.

Using these parameters of the solar model, a set of evolutionary tracks was calculated from the zero-age main-sequence (ZAMS) to the red giant branch for stars in the range of masses between 0.5 and 2.5 $M_\odot$ in steps of 0.1 $M_\odot$. The same procedure was followed for the stellar models with overshoot parameters of 0.15, 0.20, and $0.25H_p$; in the case of the $D_{\rm mix} = 0.10H_p$ models, evolutionary tracks were constructed for the mass range $1.1\ M_\odot \leq M \leq 2.5\ M_\odot$. Finally, the isochrones were derived using the modified code (Chaboyer et al. 1992) of the Revised Yale Isochrones (Green, Demarque, & King 1987) based upon an improved bolometric correction scale (Green 1988).

4.5.2. *Fitting Procedure and Results*

In the case of M67, the morphology of the main-sequence turnoff displays a prominent blue hook and a vertical gap both of which are made more pronounced by the presence of convective overshoot in the cores of turnoff stars. In order to assess the degree of overshoot that is appropriate for M67, Figures 6–9 show isochrone comparisons with $D_{\rm mix} = 0.00H_p$, $0.10H_p$, and $0.15H_p$, adopting the metallicity, reddening, and distance values discussed previously. When considering the nonovershoot and $0.15H_p$ isochrone sets, it seems that the 4 Gyr sequence best fits the data but it does not completely reproduce the morphology of the turnoff region. In particular, the color extent of the red portion of the hook is too small in the $0.00H_p$ models and too large in the $0.15H_p$ models. In contrast, the $D_{\rm mix} = 0.1H_p$ isochrones appear to be just right; thus, we conclude that the optimum comparison between the isochrones and the M67 photometry occurs for $D_{\rm mix} = 0.1H_p$ and yields an age of 4.0 ± 0.5 Gyr.

The lack of a blue hook and a vertical gap at the turnoff of NGC 188 suggests that the presence of convective overshoot is minimal or nonexistent. As such, we have chosen to perform the isochrone comparisons to NGC 188 using only the nonovershoot isochrones. These are shown in Figure 10, again utilizing the distance modulus and reddening derived earlier. In this case, we conclude that NGC 188 is 7.0 ± 0.5 Gyr old, or, stated another way, it is 3.0 ± 0.7 Gyr older than M67.

For both NGC 188 and M67, the isochrones do not reproduce the location of the red giant branch. Demarque, Green, & Guenther (1992) and Kozhurina-Platais et al. (1997) discuss the possible reasons for this. Briefly, uncertainties in the mixing length parameter, the use of the Eddington $T(\tau)$ approximation in the atmosphere, and the color transformation are all sources of error in this regard. These same uncertainties and limitations in the models, especially the final one mentioned, contribute to the inabil-

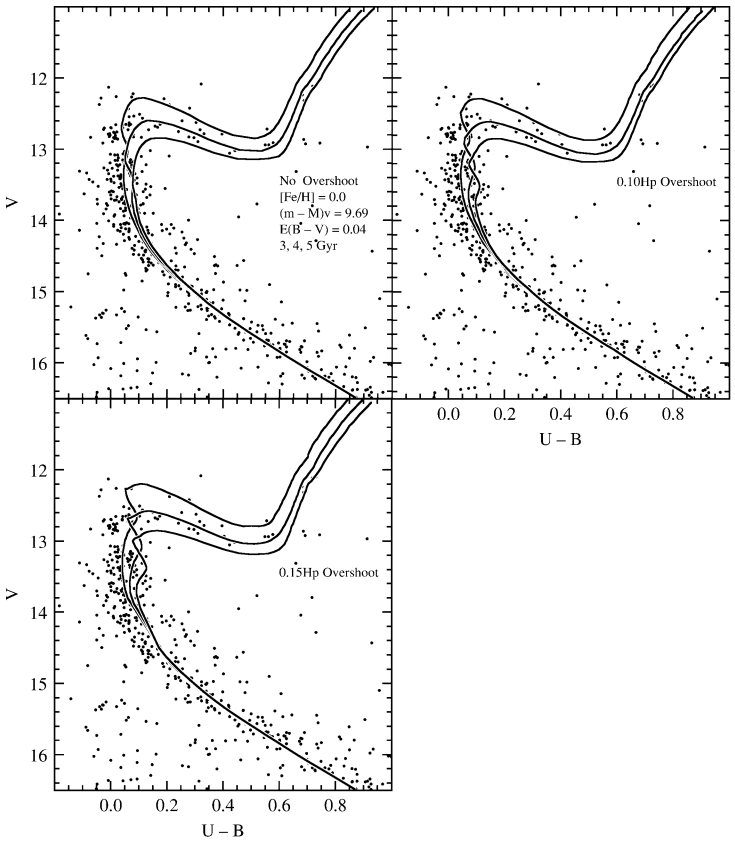

FIG. 6.—Four panels show the $U-B$ color-magnitude diagram of M67 along with theoretical isochrones computed assuming no overshoot at the edge of the convective core, overshooting in the amount of 0.1 of a pressure scale height ($0.10H_p$), and 0.15 of a pressure scale height ($0.15H_p$). The adopted metal abundance, reddening and distance are discussed in the text.

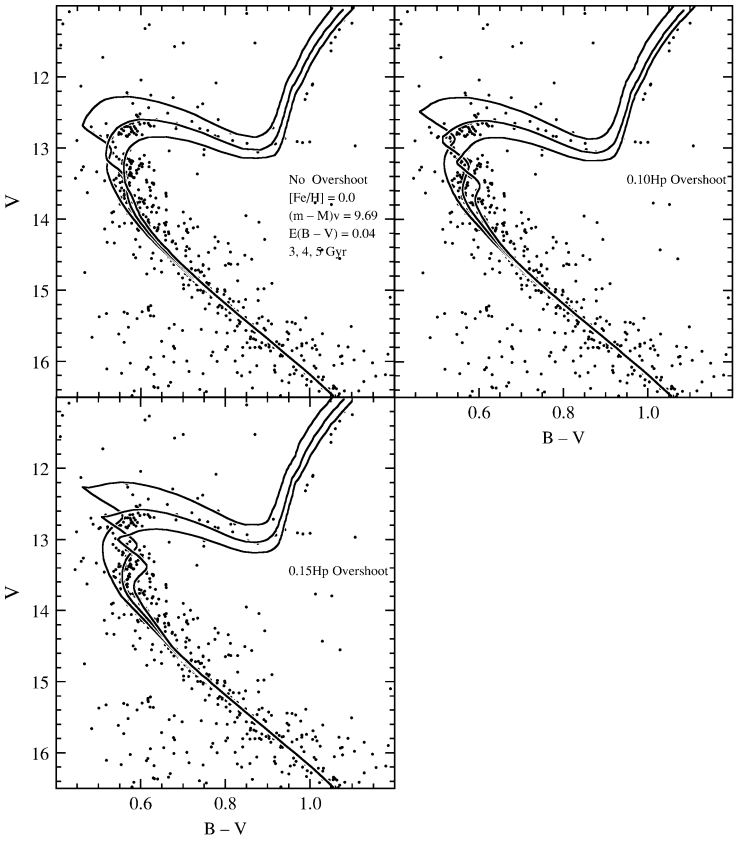

FIG. 7.—Same as Fig. 6, except that the $B-V$ color-magnitude diagram is shown

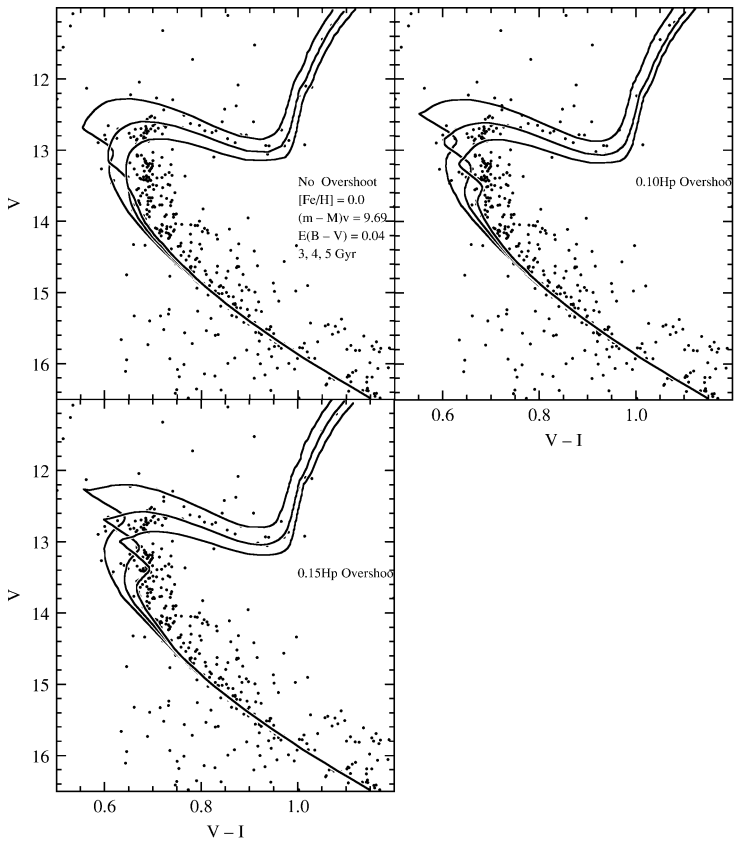

FIG. 8.—Same as Fig. 6, except that the $V-I$ color-magnitude diagram is shown

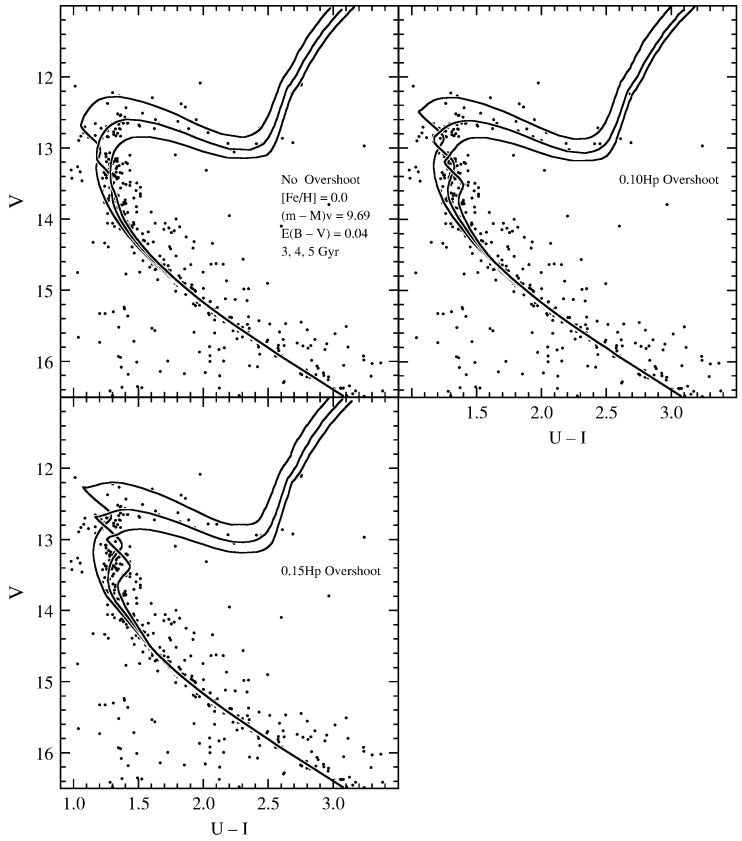

FIG. 9.—Same as Fig. 6, except that the $U-I$ color-magnitude diagram is shown

ity of the V–I isochrones to fit the observed location of the M67 turnoff.

We are in a position to draw a more comprehensive conclusion with regard to the effect of convective overshoot on cluster *ages* derived from isochrones. The upper panel of Figure 11 shows the isochrones generated by Demarque, Sarajedini, & Guo (1994) in their study of NGC 2420, while the lower panel displays the isochrones generated in this study. It is clear that while the inclusion of overshoot in the models changes the morphology of the turnoff, this effect diminishes with increasing age. For clusters older than ~ 4 Gyr, the location of the horizontal portion of the subgiant branch (HSGB; i.e., the Herzprung Gap) does not change when we include overshoot in the models. This means that the quality of the isochrone fit to the HSGB of the cluster can be used as an age diagnostic irrespective of whether overshoot isochrones are used as long as the age of the cluster is known to be older than ~ 4 Gyr.

4.6. *Mass Segregation*

In order to examine the cluster dynamical state we selected stars in the NGC 188 $V-I$ CMD along the cluster–single-star fiducial sequence. These selected stars are indicated in Figure 12. We chose the $V-I$ CMD rather than the one in $B-V$ as the color separation between the cluster and the field is better in the former. We were able to trace this sequence from $V = 11$ to $V = 19.5$. Objects were selected in a narrow range of color, within approximately $\Delta\ (V-\mathrm{I}) = 0.1$, depending on their location in the CMD. Clearly no photometric selection process will be perfect and true cluster stars will be found in the field star lists and vice versa. We chose to make the selection process as conservative as we reasonably could, necessarily selecting against cluster equal-mass binaries and blue stragglers. Although many such cluster stars are evident in the CMD they would accompany increased field star contamination, and more importantly, the bona fide cluster binaries and blue stragglers have uncertain masses. Thus, although the cluster sample that remains is incomplete in various ways, it is as close to an unbiased representation of the spatial distribution of single star cluster members as we can achieve without proper motions to $V = 19.5$. The single greatest remaining source of bias is the field stars that happen to lie along the NGC 188 fiducial sequence. Their presence, which we estimate at $\sim 20\%$ based on the number of field stars near the cluster fiducial sequence, will tend to slightly reduce the measured mass segregation. Additionally, some high mass ratio binaries still exist in this sample (see von Hippel & Sarajedini 1998) but the additional mass contribution from such secondaries is minor.

The color-selected NGC 188 members were then placed in three magnitude groups encompassing 305 stars with $11 \leq V < 16$, 348 stars with $16 \leq V < 18$, and 175 stars with $18 \leq V < 19.5$. These luminosity groups correspond to the mass ranges $M/M_{\odot} > 1.1$, $1.1 \geq M/M_{\odot} > 0.8$, and $0.8 \geq M/M_{\odot} > 0.65$, based on the empirical mass-luminosity relation of Henry & McCarthy (1993). Comparison samples were derived from the color-deselected (presumably field) stars in the same magnitude ranges. An additional comparison sample was created from a hypothetical uniform distribution that allowed us to quantitatively compare our results taking into full account the position of our cluster center on the CCD and the effects of missing field area where the larger radii are found only in

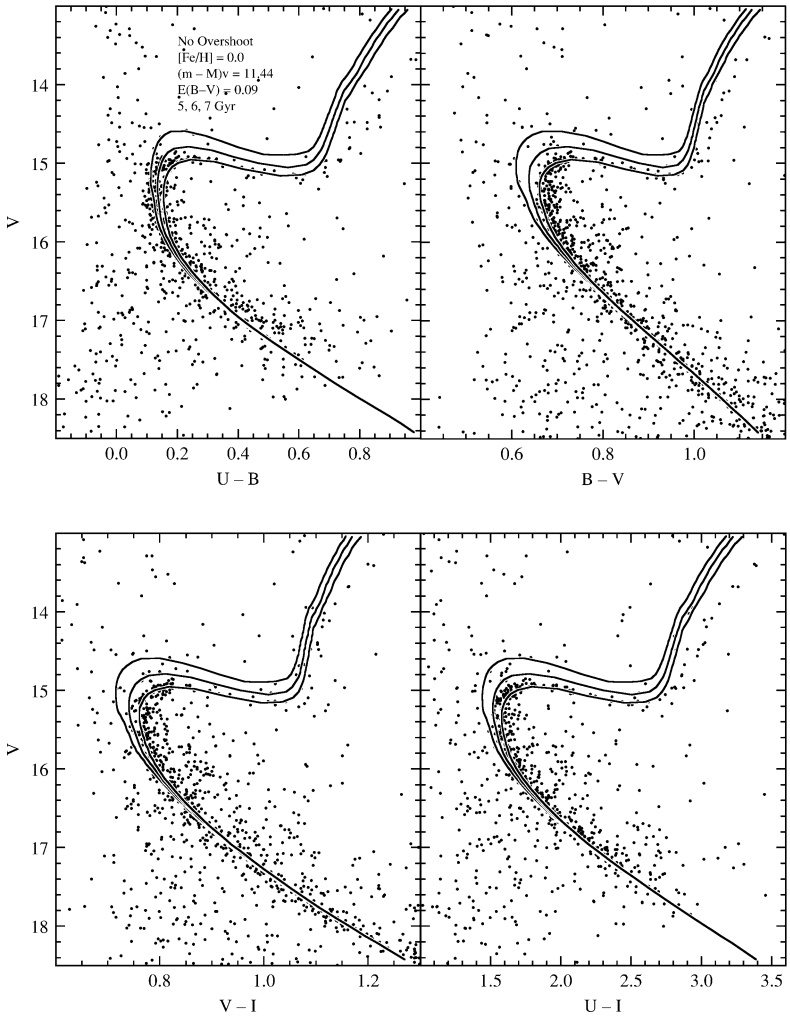

FIG. 10.—Four panels show $U-B$, $B-V$, $V-I$, and $U-I$ color-magnitude diagrams of NGC 188 along with theoretical isochrones computed assuming no overshoot at the edge of the convective core. The adopted metal abundance, reddening, and distance are discussed in the text.

the CCD corners. In order to calculate the cluster radial profiles we first had to locate the cluster center. We did this by examining a series of cluster profiles binned in the CCD x- and y-coordinates and found that the cluster center was at $x, y = 1{,}050, 900 \pm 100$. The error on the cluster position is an estimate, and corresponds to 68″. This positioning error may seem significant but our field spans 23′, and the cluster itself spans at least 1° (Dinescu et al. 1997). Any error in the cluster center would serve to decrease the measured mass segregation as stars from different true cluster radii were azimuthally averaged into the same measured radii. NGC 188 exhibits strong mass segregation, as we show below, so any error we may have made in locating the center of NGC 188 is unimportant for this study.

The cumulative radial distributions of color-selected NGC 188 members are presented in Figure 13 along with the hypothetical uniform distribution. The most massive cluster members are clearly the most centrally concentrated and all cluster members exhibit some central concentration, i.e., none of the cluster distributions are similar to the uniform distribution. The statistics of this statement will be discussed below. The cumulative radial distributions of the color-deselected field stars are presented in Figure 14. While all three color-deselected distributions appear closer to the uniform distribution than their cluster member counterparts, it is clear that the brightest luminosity group still contains a significant number of cluster members. This luminosity group likely contains both binaries along the giant branch (Green et al. 1998) and a significant number of cluster blue stragglers. Both of these components in the color-deselected group are massive cluster members, and thus significant mass segregation is expected for this brightest color-deselected sample.

In order to demonstrate statistically that the three NGC 188 samples are unlike each other, their color-deselected counterparts, or a uniform distribution we performed a series of Kolmogorov-Smirnov (KS) tests between each population. Table 3 lists the KS fractional probabilities that any two radial distribution pairs (grouped in the listed V magnitude ranges) were drawn from the same parent distribution. Columns and rows are labeled with either "cluster" or "field" indicating to which group the KS statistic refers. The brightest and most massive cluster members have less than a 0.01% chance of being drawn from the parent population of any other distribution, except for the intermediate mass cluster members, of which there is a 2.5% likelihood that they were drawn from the same parent population. As noted qualitatively above, the brightest color-deselected population has only a 0.01% chance of being drawn from a uniform distribution, whereas the

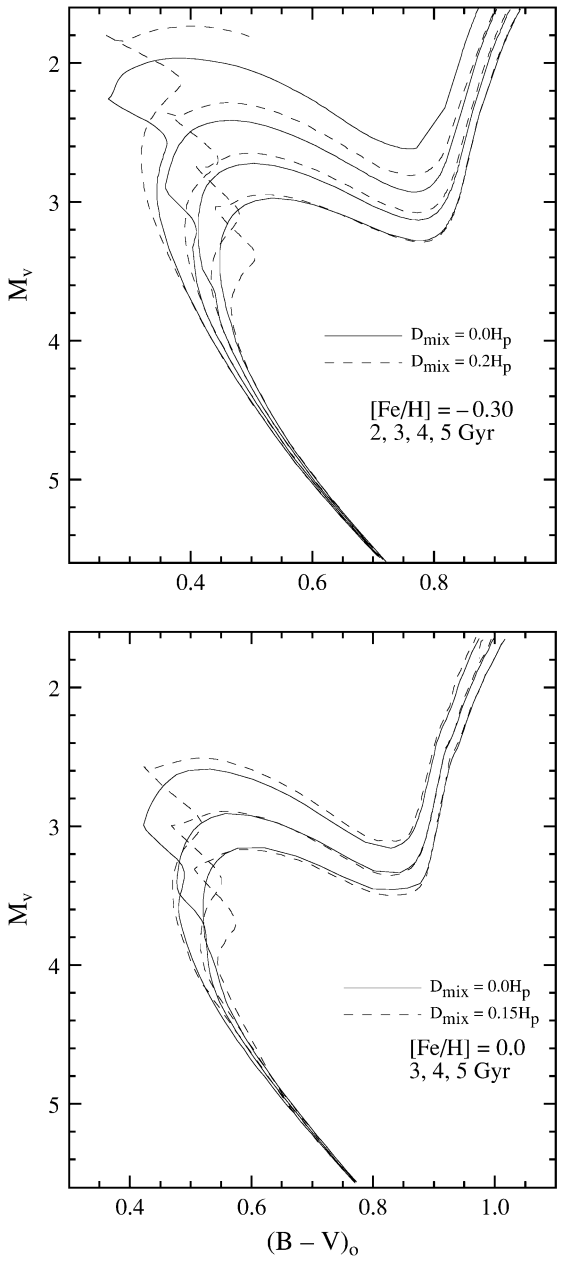

FIG. 11.—Top panel shows the isochrones generated in the study of Demarque et al. (1994) for [Fe/H] = −0.30 and the indicated overshoot values. The lower panel shows the isochrones produced in this study for solar metal abundance. It is interesting to note that for clusters older than ~4 Gyr, the location of the horizontal portion of the subgiant branch does not change when we include overshoot in the models.

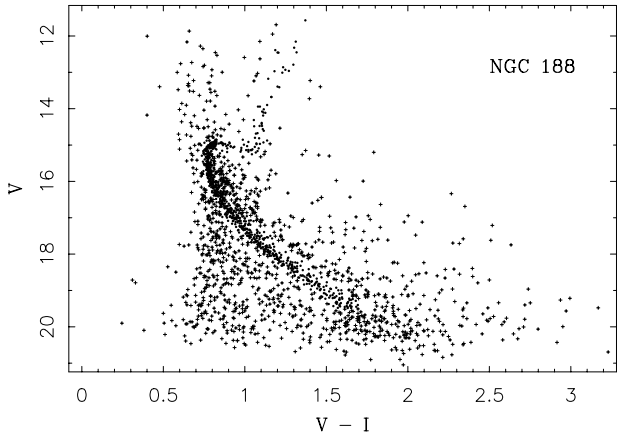

FIG. 12.—Color-selected NGC 188 stellar sequence. Selected objects are indicated by solid circles whereas nonselected objects are indicated by plus symbols.

fainter field stars are statistically consistent with being drawn from a uniform distribution.

Our analysis of NGC 188 clearly demonstrates mass segregation. How does M67, with its similar cluster mass, stellar density, and age compare? We applied the same analysis procedure described above to the *V*- and *I*-band M67 data of Montgomery et al. (1993), doing our best to take into account differences between their data set and

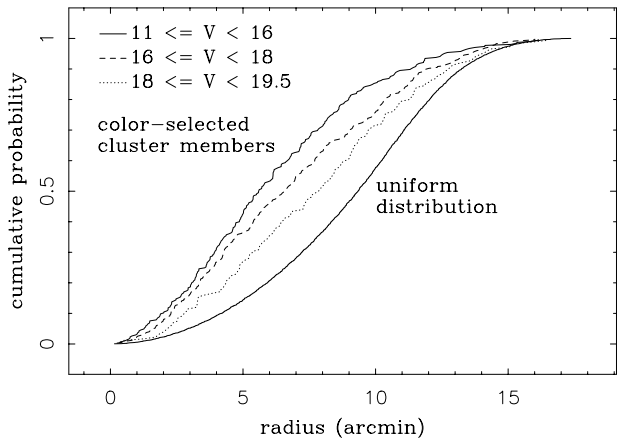

FIG. 13.—Cumulative probability of finding NGC 188 single star members at a given cluster radius. The distributions are presented for the labeled apparent magnitude bins and for a hypothetical uniform population.

TABLE 3

NGC 188 KS PROBABILITIES

	CLUSTER			FIELD			
V MAGNITUDE RANGE	11–16	16–18	18–19.5	11–16	16–18	18–19.5	NOTES
16–18	0.0250	...	...	...	...	...	Cluster
18–19.5.....	0.0000	0.0376	...	...	...	...	Cluster
11–16	0.0000	0.0198	0.8781	...	...	...	Field
1618	0.0000	0.0000	0.0137	0.0274	...	...	Field
18–19.5.....	0.0000	0.0000	0.0030	0.0060	0.4045	...	Field
Uniform	0.0000	0.0000	0.0002	0.0001	0.0266	0.6021	Field

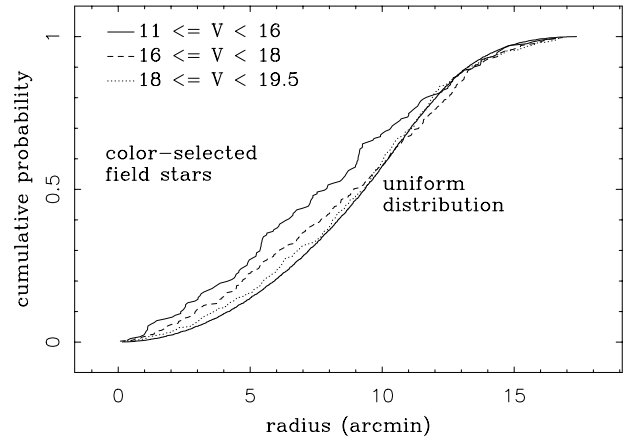

FIG. 14.—Cumulative probability of finding "field" stars within the same magnitude bins as in Fig. 13. As discussed in the text, the brightest "field" star group contains many cluster members, and as such does not display a uniform distribution.

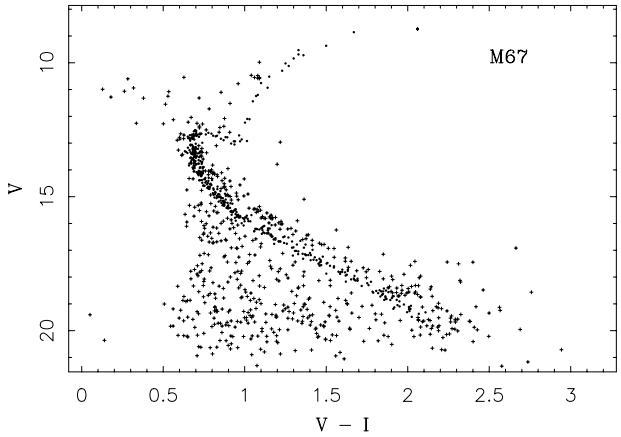

FIG. 15.—Same as Fig. 12, except for M67

ours. The Montgomery et al. photometry was obtained with the same telescope, the Kitt Peak 0.9 m, but they generally used a much smaller 512 × 512 pixel CCD, and thus they were forced to mosaic the M67 cluster field. A few CCD fields from their original 5 × 5 CCD grid were not observed in the *I*-band. Additionally, seeing differences over the period of their original three-night run undoubtedly contributed to differences in photometric depth and precision from field to field, though these differences were apparently minor.

Figure 15 shows the color-selected M67 stellar sequence. Note that M67 suffers less field contamination than does NGC 188, so this step in the analysis procedure was easier. Note also that we again purposely selected against the cluster binary sequence, blue stragglers, and the red clump near $V-I = 1.1$ and $V = 10.5$. Determining the center of M67 was more difficult since we did not know the exact distribution of the observed CCD fields, although we were able to make a reasonable guess. We found the cluster center to be at $\alpha = 8{:}48{:}43$, $\delta = +12{:}00{:}00 \pm 100$ arcseconds. We quote these in equinox 1950, as given in Montgomery et al.

The cumulative radial distributions for M67 are plotted in Figure 16. Note that the magnitude cuts are somewhat different since the distance modulus to M67 is 1.75 mag less than that of NGC 188. Since stellar mass is the intrinsic quantity we are studying here, we chose to use the same mass ranges for the M67 analysis, rather than the same luminosity range. Note, however, that since M67 is closer than NGC 188, and since the two photometry data sets probe to essentially the same depth, the stellar sample we are studying extends to 0.53 $M_\odot$ in M67 as compared with 0.65 $M_\odot$ in NGC 188. We chose not to cut off the M67 data at 0.65 $M_\odot$ since the comparable mass range in NGC 188 is significantly more contaminated by field stars, which already denies us the opportunity to make quantitative comparisons between the final mass bins of these two clusters. M67 exhibits the same mass segregation trends as did NGC 188. As with NGC 188, clearly the more massive M67 stars are the most centrally concentrated. Formally (see Table 4) the KS likelihood statistics indicate very similar significance levels to those presented for NGC 188 (see Table 3). A detailed comparison between Tables 3 and 4 should not be made, however, since we are less knowledgeable of the location of the center and any variations in the

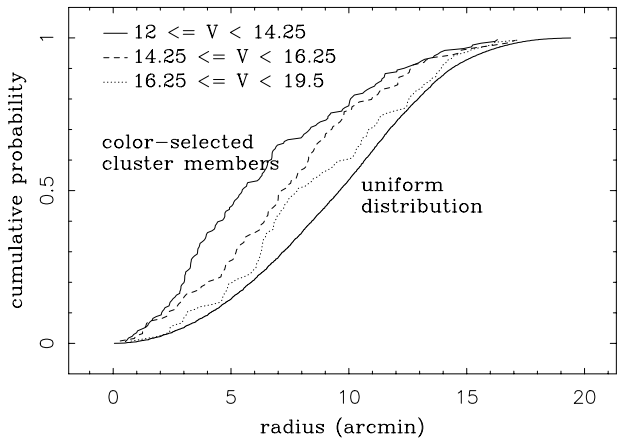

FIG. 16.—Same as Fig. 13, except for M67

TABLE 4

M67 KS PROBABILITIES

	CLUSTER			FIELD			
V MAGNITUDE RANGE	12–14.5	14.5–16.25	16.25–19.5	12–4.5	14.5–16.25	16.25–19.5	NOTES
14.25–16.25	0.0076	...	...	...	...	...	Cluster
16.25–19.5	0.0000	0.0467	...	...	...	...	Cluster
12–14.5.....	0.9892	0.0406	0.0012	...	...	...	Field
14.5–16.25	0.1580	0.8978	0.0570	0.3595	...	...	Field
16.25–19.5	0.0000	0.0000	0.0052	0.0000	0.0001	...	Field
Uniform	0.0000	0.0000	0.0024	0.0000	0.0000	0.4502	Field

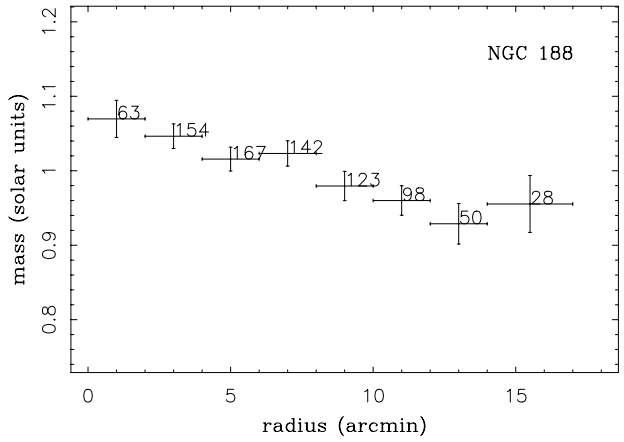

FIG. 17.—Mean mass as a function of radius for the color-selected NGC 188 members. The horizontal error bars indicate the 2′ annuli over which the mass averages were made and the vertical error bars indicate the standard error in the mean mass. The number of stars in each bin are plotted next to each point.

photometric depth of the M67 data. Nonetheless, the statistical significance of mass segregation in both clusters is high.

A different and perhaps more intuitive demonstration of mass segregation for both clusters is presented in Figure 17 for NGC 188 and Figure 18 for M67. These plots give the mean mass as a function of cluster radius for the color-selected cluster members. We convert the V-band photometry to mass values following the empirical relations of Henry & McCarthy (1993). For NGC 188, we transform the main-sequence photometry to mass in the range $15.2 \leq V \leq 19.5$, corresponding to $3.76 \leq M_V \leq 8.06$ for our distance modulus, $(m - M)_V = 11.44$. Cluster stars brighter than 15.2, i.e., those from the turn-off through the red giant branch tip, are assumed to have a mass of 1.28 $M_\odot$. Although we expect an increase in mass with luminosity up the giant branch of $\approx 0.1\ M_\odot$, this small change coupled with the limited number of cluster giants insignificantly affects our derived mean mass at any radius. For M67 we transform photometry to mass in the range $13.07 \leq V \leq 19.5$, corresponding to $3.38 \leq M_V \leq 9.81$ for our distance modulus, $(m - M)_V = 9.69$. Cluster stars brighter than 13.07 up to 12.00 (the brightness limit of the Montgomery et al. data), i.e., those from the turn-off

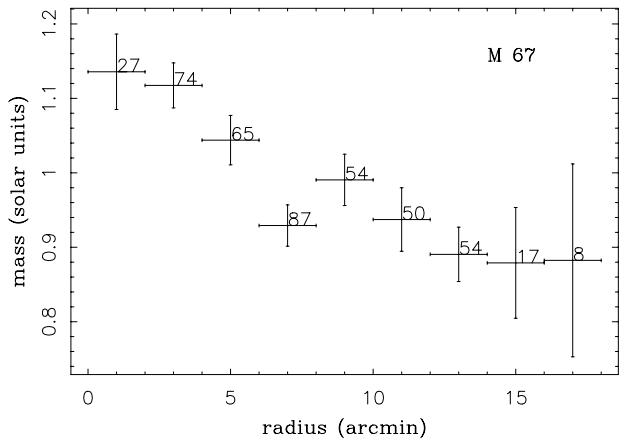

FIG. 18.—Same as Fig. 17, except for M67

through the subgiant region, are assumed to have a mass of 1.39 $M_\odot$. Note that both clusters are plotted with the same axis scaling. There is a clear decrease in the mean mass of both NGC 188 and M67 cluster stars with radius. The trend in M67 is significantly stronger, $\sim 0.2\ M_\odot$ over 18′, compared with $\sim 0.1\ M_\odot$ over 17′ for NGC 188. We attribute the greater apparent mass segregation in M67 partially to the real effect of the greater mass range in M67 and partially to the observational effect of the increased field contamination in NGC 188.

5. CONCLUSIONS

We present high-precision $UBVRI$ CCD photometry of a 23 × 23 arcmin field centered on the old open cluster NGC 188. Our color-magnitude diagram extends from near the red giant branch tip to as faint as ~ 5 mag below the main-sequence turnoff. From analysis of these data and similar photometry of M67 from Montgomery et al. (1993), we draw the following conclusions.

1. Consistent with the results of Paper I, there is a significant offset between the photometric zero point of the present paper and that of Eggen & Sandage (1969). This is important to note because all previous photometric studies of NGC 188 before Paper I used the Eggen & Sandage (1969) photometric scale.

2. From the UBV two-color diagram, we find a reddening of $E(B-V) = 0.04 \pm 0.02$ for M67 and $E(B-V) = 0.09 \pm 0.02$ for NGC 188.

3. Based on main-sequence fitting to solar abundance isochrones, the distance moduli turn out to be $(m - M)_v = 9.69 \pm 0.11$ for M67 and $(m - M)_v = 11.44 \pm 0.08$ for NGC 188. If we were to adjust these moduli for the slightly lower-than-solar metallicities of these clusters, $[\mathrm{Fe/H}] = -0.05 \pm 0.08$ for M67 and $[\mathrm{Fe/H}] = -0.04 \pm 0.05$ for NGC 188, then $+0.055$ mag and $+0.044$ mag, respectively, must be subtracted from the distance moduli.

4. The comparison of the CMDs to theoretical isochrones indicates that an amount of core convective overshoot equivalent to 0.10 of a pressure scale height is appropriate for M67, while no overshoot is required to fit the CMD of NGC 188. These isochrones yield an age of 4.0 ± 0.5 Gyr for M67 and 7.0 ± 0.5 Gyr for NGC 188, or, stated another way, NGC 188 is 3.0 ± 0.7 Gyr older than M67.

5. There is a clear indication of mass segregation in both M67 and NGC 188 with the most massive stars ($M/M_\odot > 1.1$) being more centrally concentrated than the least massive ones ($0.8 \geq M/M_\odot > 0.65$). This phenomenon is demonstrated through the use of cumulative radial distributions for stars with a range of masses as well as examination of the mean mass as a function of radius in each cluster.

Much of this work was performed while A. Sarajedini was a Hubble Fellow at Kitt Peak National Observatory and San Francisco State University and was supported by the National Aeronautics and Space Administration (NASA) grant number HF-01077.01-94A from the Space Telescope Science Institute, which is operated by the Association of Universities for Research in Astronomy, Inc., under NASA contract NAS 5-26555. Additional support has been provided by the National Science Foundation under grant AST 98-19768.

REFERENCES

Alves, D. R., & Sarajedini, A. 1999, ApJ, 511, 225
Boesgaard, A. M., & Friel, E. D. 1990, ApJ, 351, 467
Caputo, F., Chieffi, A., Castellani, V., Colados, M., Martinez Roger, C., & Paez, E. 1990, AJ, 99, 261
Cardelli, J. A., Clayton, G. C., & Mathis, J. S. 1989, ApJ, 345, 245
Chaboyer, B., Deliyannis, C. P., Demarque, P., Pinsonneault, M. H., & Sarajedini, A. 1992, ApJ, 388, 372
Chaboyer, B., Green, E. M., & Liebert, J. 1999, AJ, 117, 1360
Cole, A. A. 1998, ApJ, 500, L137
Demarque, P., Green, E. M., & Guenther, D. B. 1992, AJ, 103, 151
Demarque, P., & Larson, R. B. 1964, ApJ, 140, 544
Demarque, P., & McClure, R. D. 1977, in The Evolution of Galaxies and Stellar Populations, ed. B. M. Tinsley & R. B. Larson (New Haven: Yale Univ. Obs.)
Demarque, P., Sarajedini, A., & Guo, X. J. 1994, ApJ, 426, 165
Dinescu, D. I., Girard, T. M., Van Altena, W. F., Yang, T.-G., & Lee, Y.-W. 1997, AJ, 111, 1205
Eggen, O., & Sandage, A. 1969, ApJ, 158, 669 (ES69)
Green, E. M. 1988, in Calibration of Stellar Ages, ed. A. G. D. Philip (Schenectady: Davis), 81
Green, E. M., Demarque, P., & King, C. R. 1987, Revised Yale Isochrones and Luminosity Functions (New Haven: Yale Univ. Obs.)
Green, E. M., et al. 1998, BAAS, 192, 6713
Henry, T. J., & McCarthy, D. W. 1993, AJ, 106, 773
Hoyle, F. 1959, MNRAS, 119, 124
Iben, I. 1967, ApJ, 147, 624
Kaluzny, J. 1990, Acta Astron., 40, 61
Kozhurina-Platais, V., Demarque, P., Platais, I., Orosz, J. A., & Barnes, S. 1997, AJ, 113, 1045
Landolt, A. U. 1992, AJ, 104, 340
Landsman, W., Bohlin, R. C., Neff, S. G., O'Connell, R. W., Roberts, M. S., Smith, A. M., & Stecher, T. P. 1998, AJ, 116, 789
Montgomery, K. A., Marschall, L., & Janes, K. A. 1993, AJ, 106, 181
Phelps, R. L. 1997, ApJ, 483, 826
Sandage, A. 1962, ApJ, 135, 349
Sarajedini, A. 1999, in press
Sarajedini, A., & Da Costa, G. S. 1991, AJ, 102, 628
Sarajedini, A., & Milone, A. A. E. 1995, AJ, 109, 269
Sarajedini, A., Lee, Y.-W., & Lee, D.-H. 1995a, ApJ, 450, 712
Sarajedini, A., Davis, L., Carder, E., Kinman, T., & Jacoby, G. 1995b, NOAO Newsl. 43
Schlegel, D. J., Finkbeiner, D. P., & Davis, M. 1998, ApJ, 500, 525
Schmidt-Kaler, T. H. 1982, in Stars and Star Clusters, ed. K. Schaifers, H. H. Voight, & H. Landolt (Berlin: Springer), 1
Seidel, E., Demarque, P., & Weinberg, D. 1987, ApJS, 63, 917
Stetson, P. B. 1994, PASP, 106, 250
Twarog, B. A. 1978, ApJ, 220, 890
Udalski, A. 1998, Acta Astron., 48, 383
Vassiliadis, E., & Wood, P. 1993, ApJ, 413, 641
von Hippel, T., & Sarajedini, A. 1998, AJ, 116, 1789